



## Biomaterials & Architecture; a Possible Future: Bio Printing Architecture

Alberto T Estevez<sup>1</sup>, Yomna K Abdallah<sup>2\*</sup>

<sup>1</sup>Department of Architecture, IBAG-UIC Barcelona, Institute for Biodigital Architecture & Genetics, Universitat Internacional de Catalunya, Barcelona, Spain

<sup>2</sup>Department of Interior Design, Helwan University, Cairo, Egypt

\*Corresponding author: Abdallah YK, Department of Interior Design, Helwan University, Cairo, Egypt; Email: yomnaabdallah@uic.es

Received: 08-March-2022, Manuscript No. JRGM-22-001;

Editor assigned: 11-March-2022, PreQC No. JRGM-22-001(PQ);

Reviewed: 25-March-2022, QC No. JRGM-22-001;

Revised: 30-March-2022, Manuscript No. JRGM-22-001(R);

Published: 05-April-2022, DOI: 10.4172/2325-9620.1000210

### Abstract

The Zeitgeist of the time we live in deserves that we give it feedback, and it is about time we start to do so. We, the inhabitants of the twenty-first century, should start to design “from DNA to the planet” with the commitment to achieve sustainability. We are witnessing the rapid advancement in sustainable building materials and fabrication tools. These materials are self-healing, autonomous, and morphogenetic. Thus, possessing an inherent capacity to remodel themselves in response to their surrounding environment using the minimum resources, and depositing density and strength in response to various mechanical stimuli. This is what bio mineralization in bone tissue performs on a micro-deposition scale. Thus, in the current work, we employ a bio-inspired model of bio mineralization and extrusion bio printing to propose autonomously bio mineralized materials. Here, the integration of osteosarcoma (Saos-2) cells, encapsulated in GelMA hydrogel, is proposed to enable their growth, differentiation, and bio mineralization, as a proof of concept. This is proved through the effect of the geometrical design on cell viability, through comparing the shape fidelity and biocompatibility between three different geometrical designs. The results revealed that the orthogonal square plan geometry achieved the highest cells viability and shape fidelity followed by the deferential growth pattern.

**Keywords:** Living architecture; Bio mineralization; Bio printing; Micro-spatial deposition control; Saos-2

### Introduction

Nowadays, sustainability is an essential requirement in the architectural built environment; achieved by construction systems or materials or both. This interchange between materials and construction systems was always managed by solutions based on uniform-density systems. In structural efficiency, the density at each point of a volume

is responsible for load-bearing, and resistance at this point, thus defining how much material is needed at this specific point. This interplay between how much material and what construction method is used to achieve sustainability is also a time-dependent equation, not just in terms of the concurrent effect of physical and natural forces over this material structure, but also dependent on the advancement in the methods and tools of material engineering and architectural construction. Consequently, the current and future built environment demands more than a static solid material. It demands a material that is autonomously remodeling itself exactly where needed, self-healing, regenerating, growing, and differentiating in response to its inner and surrounding environment.

Automation and regeneration of synthesized materials in general and building materials specifically have attracted the attention of many researchers lately. Through bioengineering, the research community has been attempting to synthesize a material that acts as a living being that is able to grow, self-heal, and respond to different stimuli [1]. And in the architecture realm, this has been a long-awaited dream, to achieve the living architecture, either by robotizing its parts, exploiting artificial intelligence to respond as a living being, or by integrating bioactive agents –cells or parts of them–in these materials to perform different physiological pathways translated as eco-functioning architectural systems [2]. However, these attempts were all conducted in light of available design and fabrication tools, and today, these tools are rapidly developing and opening further potential for realizing this living material and living architecture.

Nowadays, having the promising potential of the digital design and fabrication tools, especially advanced 3D printing, and bio printing enabled the customization of the design and fabrication of synthetic materials, managed by solving the material composition, the printing technique, and the form physiology or in other words the geometrical composition of the material structural design. To solve this multi-parameter equation, in the current work, a bio learning approach was adopted to follow a simplified model of bone tissue and integrate its bio agents into this bio manufacturing process to realize a living synthetic material. In this case, bone tissue is the optimum natural reference to self-healing, regenerative, and morphogenetic material synthesized with high precision and locating material exactly where needed achieving optimum formal physiology of a structure. In the current work, bone cells, optimum bionic composition, and extrusion bio printing were employed to manifest the emergence of a bio printed living architecture made of bone cells, justifying its future potential and fields of application.

Through this proof of concept, 3D bio printed different architectural models with different geometrical complexities will be exhibited. This will be achieved with the optimized geometrical design, the bionic composition, and 3D extrusion bio printing. Proving the formal design biocompatibility by testing the effect of the geometrical composition on cell viability for different prints. Thus, the paper will begin by explaining the formal physiology of natural bone tissue, justifying the use of bone cells as the bioactive agent in this proposed material by analyzing the bone tissue structure and the bio mineralization process. Followed by a comparison between material structures and structural materials and how bone tissue achieves the characteristics of both categories. Then, the proof of concept manifesting the achievability of this practice, on a pilot scale, and exhibiting the results of different geometrical compositions on achieving formal physiology.

## Literature Review

### Bone tissue efficiency

Bone tissue is the key reference in this study due to its highly efficiency and regenerative form. As it performs as structural, shield and dynamic system in the human body. This system controls locomotion; protect soft tissues, and store bone marrow, calcium and phosphate [3]. The key characteristic of bone is the customized material distribution orchestrated by the bio mineralization process that guarantees the formation and regeneration of bone tissue accurately where needed, ensuring material sustainability and durability. This is called "Micro Spatial Deposition Control," giving the bone tissue its unique structural pattern that is highly effective in delivering its function.

To understand the formal physiology of bone structure, a reference to the bio mineralization process is provided, defining bone as a mineralized tissue that is composed from the orchestrated collaboration of the bone lining cells, osteoblasts, osteocytes, and osteoclasts [4]. Bone tissue is continuously absorbed by osteoclasts and regenerated by osteoblasts, regulated by the role of osteocytes as Mechano-sensors of this bone remodeling process [5]. This bone regeneration is achieved in a three-step cycle. First, the osteoclasts initialize the bone resorption. Then, the osteoblasts perform the transition from resorption to new bone formation, and lastly, the new bone is formed by the osteoblasts [6,7]. This bone regeneration is responsible for healing, adaptation to mechanical functions, and calcium homeostasis [8,9]. This definition reveals two more important characteristics of bone customized material deposition: self-healing and continuous growth (morphogenesis). This equilibrium between new bone formation and old bone resorption is controlled by several local and systemic factors, including mainly biomechanical stimulation [10].

In essence, the regeneration of bone includes sequence of processes that are cell and protein-mediated, including the development of a protein-based organic matrix that is followed by cellular deposition of osteoid, which crystallizes on the matrix under the control of the comprising proteins [11-14]. These processes rule the definition of the micro spatial control of bone tissue generation [15].

Tissue engineering is one of the main approaches to micro spatial control of bone generation, through the integration of various estrogenic constituents into biomaterials. For example, previous studies used bone-derived proteins and ground seashell incorporated into Polyethylene Glycol (PEG) hydrogels to perform bone generation in macroscopic patterns [16,17]. However, in this work congruent with exploiting the natural bioactive agents to perform their physiological pathways in bone generation and bio mineralization, we opt to use osteosarcoma cells to employ their activity in bio mineralization in synthesizing the desired bioactive material. To break down this process, an explanation of the different types of bone cells involved in this process is given in the following section.

Since, osteoblasts are known as bone forming cells [18], they exhibit morphological characteristics of protein-synthesizing cells. As they encompass ample rough idioplasmic reticulum, protuberant Golgi apparatus, and various secretory vesicles [19]. As their polarized morphology suggests, the osteoblasts exert the osteoid to the bone matrix [7]. Originally, osteoblasts are derived from Mesenchyme Mtem Cells (MSC), which indicates the expression of specific genes following a specific chronological order that includes the synthesis of

Bone Morphogenetic Proteins (BMPs) [20,21]. A proliferation phase of pre-osteoblasts occurs consequently after the synthesis of osteoblast progenitors during osteoblast differentiation. In this phase, osteoblast progenitors are considered pre-osteoblasts as they exhibit Alkaline Phosphatase (ALP) activity [18,21,22].

Consequently, the osteoblasts synthesize the bone matrix by the deposition of organic matrix and its subsequent mineralization. The organic matrix is formed by the secreted collagen proteins, non-collagen proteins, and proteoglycan. Subsequently, the bone matrix mineralization occurs by the vesicular and the febrile phases [23]. The vesicular phase occurs when portions of the matrix vesicles are released from the apical membrane of the osteoblasts into the new bone matrix; there they bind to proteoglycans and other organic components. Then, the negatively-charged sulfated proteoglycans immobilize calcium ions stored within the matrix vesicles [24]. These calcium ions are released from the proteoglycans by the degradation enzymes that are secreted from the osteoblasts. Then, they (calcium ions) cross the calcium channels in the matrix vesicles membrane [23]. On the other hand, the ALP secreted also by the osteoblasts degrades the phosphate-containing compounds to release the phosphate ions inside the matrix vesicles. Then, the phosphate and calcium ions bind to form the hydroxyapatite crystals [25]. When the super saturation of calcium and phosphate ions inside the matrix vesicles causes their rupture, the hydroxyapatite crystals spread to the neighboring matrix, which is known as the febrile phase [26].

On the other hand, osteocytes, which are the regulators of bone resorption and regeneration, are the most abundant cells as they comprise 90-95% of the total bone cells [27]. These cells are situated within lacunae enclosed by the mineralized bone matrix. These cells show differentiated dendritic morphology that differs according to the bone type, for example, osteocytes from trabecular bone are more rounded than osteocytes from cortical bone, which have an elongated morphology. Osteocytes are derived from MSCs lineage through osteoblast differentiation at the end of a bone formation cycle. Through this process, noticeable morphological and ultra-structural changes occur including the reduction of the osteoblast size, the decrease of the number of organelles, and the increase of nucleus-to-cytoplasm ratio, in response to the reduction in protein synthesis and secretion. In order for osteocytes to perform as Mechano-sensors, their interconnected network sense mechanical pressures and loads, thus, facilitating the adaptation of bone to various mechanical forces. In this way, the osteocytes orchestrate the bone regeneration or deposition by regulating osteoblast and osteoclast performance. Furthermore, osteocyte programmed cell death performs as a chemotactic signal to the resorption of the osteoplastic bone. This mechanosensitive function of osteocytes is accomplished due to their deliberate location within the bone matrix. Thus, their morphology and spatial order are congruent with their sensing and signal transport functions, by translating mechanical stimuli into biochemical signals, which is called the piezoelectric effect.

To this extent, the essential roles of Osteoblasts and Osteocytes in bone formation, regeneration, and mineralization are exhibited, complying only to the brief introduction that is essential to conduct the proof-of-concept experimental study, as well as identifying the key characteristics in natural bone bio mineralization that correspond to the required characteristics in the bioengineered model of the developed material.

In the following section, a deferential comparison between structural materials and material structure will be presented to identify

the significance of bioengineered materials as building materials, able to self-heal, adapt, and regenerate in response to changes in environmental conditions as natural bone tissue does.

### Structural Materials vs. Material Structure

Structural materials are loadbearing materials that resist external forces, and are used in the design and manufacturing of a structural framework, exhibiting multiple examples starting from clay in the form of bricks, wood, iron, concrete, and the list goes on [28]. The common characteristic of all these current and future proposed materials is their physical and chemical properties that confirm their durability and resistance to different physical and chemical effectors. Looking deeply into the physical characteristics of a material and analyzing how they evolved; it is axiomatic to say that these originate from the material chemistry; from its chemical structures based on atomic bonding and chemical composition. Atomic bonding is defined as the attraction between elements within a material matrix [29], while the chemical composition of a material is the amount of each element in this material matrix. The atomic bonding and the chemical composition together shape the organization of the material matrix within a lattice structure. The pattern of this lattice structure within a material matrix is the ruling factor in classifying all materials. These patterns are either crystalline structures or amorphous structures. If the lattice structure is repeatable and intersecting, it is categorized as a crystalline structure, including various positioning and sorts of crystals. Crystalline structures result in microstructures which are grains distributed in uniform sections of the lattice surrounding the individual grains called grain boundaries. If the lattice is arranged in a random structure, it is amorphous. The type of chemical bonds that binds the material components and how their atoms and molecules are organized also defines the standard physical properties of the material, as the distance between its molecules defines the degree of solidity, viscosity, and density of the material. This implies that what qualifies material as a structural material is its own microstructure (of the material itself). Applying this shift to focus on the material as the core structure, not as a physical mediator to translate another structural design, the structural design and material customization are fused in a one-step process, designing and synthesizing the material microstructure.

Applying this concept of the material chemical structure to material biochemical complexity, in tissue formation, the microstructure of any tissue emerges from the interactions between the cells and their Extracellular Matrix (ECM). These interactions are also essential in the physiological pathways of various biological processes [30], including development, healing, and regeneration. The mechanisms of cells' response to the mechanical properties of the ECM have been studied and simulated extensively, by integrating cells into materials with tunable stiffness's, including synthetic polymers and natural proteins. These techniques often aim to empirically define the limits of stiffness that cells experience in their interactions with the ECM and measure how cells and tissues respond phenotypically.

In the following section, a proof-of-concept will be exhibited; reporting an empirical study on developing 3D printed models of Osteosarcoma cells in GelMA hydrogel while testing the geometrical composition of this material structure on cell viability.

### Proof of Concept (Bio printed Architectural Models)

In this section, pilot-scale experimentation on bio printed architecture will be exhibited, from a housing unit, a building block to the urban tissue. These are exhibited to prove the effect of geometrical composition and scale on cell viability in the bio printed model, as an initial step to propose this living material as a futuristic building material that can perform autonomous bio mineralization by customized formal physiology and 3D printing micro-deposition.

Bio mineralization has exhibited before, is the key process in bone regeneration, self-healing, and micro deposition [31]. Thus, bone tissue engineering aims to simulate its extracellular matrix and the different biochemical pathways that are involved in the bone regeneration [32]. Employing the extrusion 3D bio printing of cell-laden hydrogels in the design and fabrication of these 3D synthesized environments that resemble natural tissues. These hydrogels are developed for diverse bionics, which are composed of polymeric hydrogels encapsulating the living cells. In this process, multi parameters from three different categories are synergized to achieve the optimized results in cell viability and activity rates. These parameters are exhibited in (Figure 1).

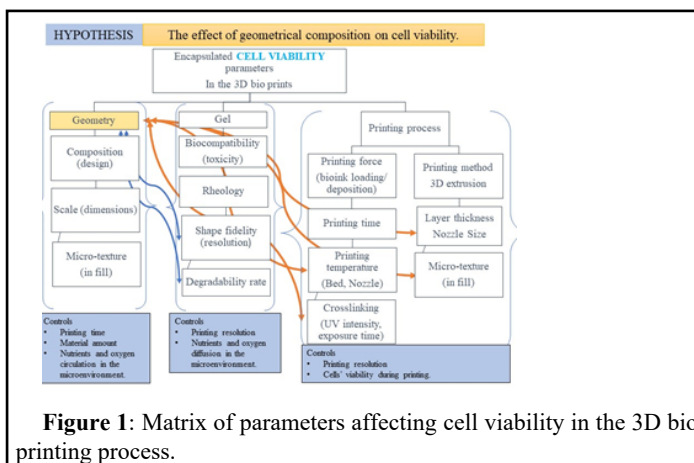


Figure 1: Matrix of parameters affecting cell viability in the 3D bio printing process.

As shown in (Figure 1), Testing the effect of geometrical composition on cell viability in terms of; geometrical dimensions, printed layer width, printed layer thickness, layer porosity, infill pattern, and scale relevance to cell dimensions and real full-scale architecture. The study will also test the effect of geometrical composition on increasing the surface area of the bio prints while maintaining cell viability during and post-printing. These parameters are interconnected with the hydrogel chemical and rheological properties; as biocompatibility (toxicity), viscosity, and plasticity, while at the same time they are also affected by the printing process settings, as the printing time, the applied pressure, printing temperature, cross-linking settings (UV light intensity and exposure duration). All these parameters are interdependent and controlled by the cell viability criteria: oxygen and nutrients circulation, the distance between cells, layer thickness, printing time, incubation period, temperature, and UV exposure. Thus, the materials and methods will be presented following this order: cell, gel, geometry, and printing process. Exhibiting at each section, the corresponding conducted tests.

### Materials and Methods

**SaOs-2 cell culture:** The (Saos-2) osteosarcoma cell line was obtained from ATCC (USA) and cultivated, following the reference of

the supplier and the method of PAUTKE, et al. 2014, in DMEM containing McCoy's 5 a medium supplements with 15% FBS and 1% penicillin/streptomycin (Sigma-Aldrich). Cells were cultivated in T25 flasks (Nunc, USA) in a humidified incubator at 37°C, using a standard mixture of 95% air and 5% CO<sub>2</sub>.

After trypsinization, the cells in suspension were morphometric ally analyzed. The phase-contrast microscope was used to measure the area and diameter of attached cells (n=100), by using an image analysis system Eclipse TS2 (Nikon, Germany). Detached cells were analyzed by staining 10 µl of the cell suspension with 10 µl of Trepan Blue solution. The cells were then counted with a Neuburger chamber (place).

For cell proliferation analysis, Saos-2 cells were seeded at 2.5 × 10<sup>5</sup> cells/T25 flask. On days two, four, eight, and fourteen, cells were detached, and their number was determined following the previous method. All assays were performed in triplicate, using the early log-phase to calculate the population replication time.

**GelMA preparation, crosslinking, and toxicity assay:** GelMA or Gelatin Methacrylate was prepared according to the traditional method of Van Den Buckle et al. 2000, based on the direct reaction between gelatin and meth acrylic anhydride (MA). The preparation process included the following steps, respectively: 1) dissolving 10% gelatin in a phosphate-buffered saline (1 × PBS: 5 tablets/1000 ml distilled water, pH=7.4) at 50-60°C. After being completely dissolved, 5% (2.5 ml) of MA (methacrylate) was added to the solution by 0.5 ml/min rate and stirred for one hour at 50°C. 2) After one hour, 200 ml of PBS was added to the solution at 40°C to stop the reaction. Then, a dialysis membrane was used to remove toxic and unreacted MA from the diluted solution. Once the dialysis was complete, ultrapure water was added to the dialyzed solution. Finally, the resultant solution was freeze-dried for storage.

Cross-linking of GelMA by radical polymerization *via* photo initiation was conducted in an aqueous medium with the water-soluble photo initiator, Irgacure 2959: 1-[4-(2-hydroxyethoxy) phenyl]-2-hydroxy-2-methyl-1-propan-1-one. GelMA (1.5 g) was liquefied in 10 mL of distilled water at 40°C containing 6 × 10<sup>-4</sup> g of photo initiator (0.042% w/w to protein concentration). Then, the warm mixture was dispensed into a cast made of two glass plates divided by a 1 mm thick silicon spacer and left to cool down to the room temperature for direct exposition to 365 nm UV light (10 mW/cm<sup>2</sup>) for seven minutes. The cast was stored at 4°C, to produce a flexible 1 mm thick transparent film.

To perform the Alamar Blue Direct Cell viability assay, three wells were seeded with 1.0 × 10<sup>4</sup> SaOs-2 cells in standard McCoy medium/well and incubated for 24 h before toxicant addition. Media within seeded wells were replaced with 100 µl of GelMA. While 1.0 × 10<sup>4</sup> SaOs-2 cells in 100 µl plasma-treated polystyrene TCP was used as a control group. SaOs-2 cells were exposed to the toxicants for 72 h before the addition of 10 µl of Alamar Blue dye. All plates were incubated for 4 h before reading on a fluorescent plate reader at 570 nm emission and 585 nm emission wavelengths. Three independent replicates of the described procedure were performed [33].

**Geometry:** Three digital designs of different geometrical compositions were designed within the domain of a 5 cm petri dish, using algorithmic aided design software Rhinoceros Grasshopper 3D. The three designs addressed three levels of the architectural built environment: a house of 1 cm × 1 cm and 1.5 cm height, a housing block of 2 cm × 2 cm by 0.5 cm height, and an urban or city design

(width per line 0.3 cm × height 0.5 cm, expanding all over the 5 cm petri dish area). The house and the housing blocks were generated from simple geometries. The urban fabric was designed by a form-finding simulation that employs a differential growth algorithm generated by the physical solver of Kangaroo Plugin in Rhinoceros Grasshopper. The three digital designs were then 3D printed in PLA using a Felix desktop 3D extrusion printer. Figure 2 exhibits the three 3D printed architectural models corresponding to the three digital designs and their architectural and urban scale.

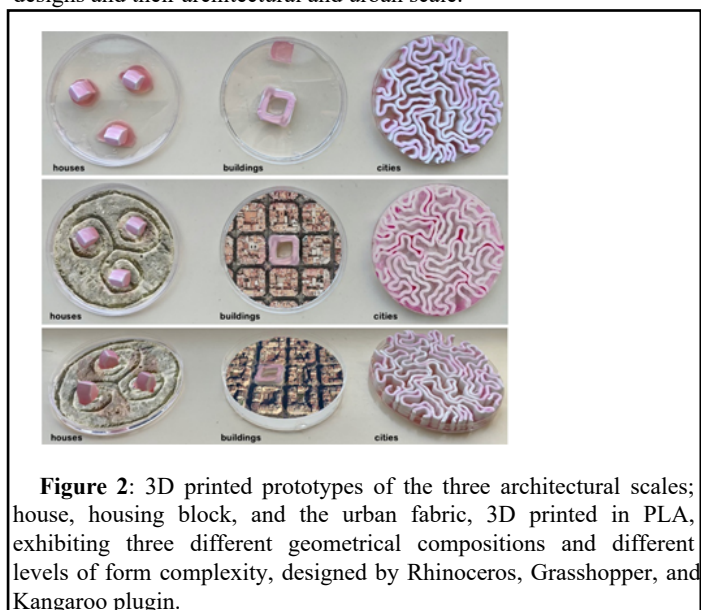


**Figure 2:** 3D printed prototypes of the three architectural scales; house, housing block, and the urban fabric, 3D printed in PLA, exhibiting three different geometrical compositions and different levels of form complexity, designed by Rhinoceros, Grasshopper, and Kangaroo plugin.

**Printing process:** The preparation for the bio printing process begun with SaOs-2 cells encapsulation in GelMA. The following procedures were followed first to detach the SaOs-2 cells to prepare them for encapsulation; old cell culture media were removed, and the cells were washed twice with 5-10 ml of PBS to remove any residues from the old media; 5-10 ml Trypsin was added to the cells and incubated for 5 minutes at 37°C to detach the cells. After incubation, the cells in Trypsin were centrifuged for 5 minutes at 300 g, and then 500 µl of McCoy medium was added to the three falcons to suspend the cells. 20 µl of cell suspension was added to 80 µl of Trepan Blue to be counted by the Neuburger chamber. After counting the cells in each falcon, the cells were placed again in three T25 flasks, and 8.1 ml of McCoy medium was added to suspend the cells at 37°C at each flask respectively, followed by the addition of 1.5 ml of the prepared GelMA through a filter to prevent bacterial infection 3 mg of Irgacure 2959. The mixture was incubated for five minutes at 37°C. All procedures were conducted in a UV sterile hood. After incubation, each mixture was loaded to a 5 ml sterile syringe and fixed into the printing head of the BioX (Cell Ink) triple head extrusion bio printer. The printing temperature was adjusted to 4°C at the printing bed and 37°C at the printing head (nozzle). All 3D digital design files were exported as STL files from Rhinoceros 3D and adjusted to printer settings using Simplify 3D software, and then transferred to the printer's built-in software. The printing settings were as follows; nozzle diameter 0.3 mm, layer height 0.3 mm, Printing pressure 12 PSI, infill pattern: rectangular grid, flow rate: 100%. After printing each of the three different designs, each print was cross-linked by exposure to 365 nm UV of 80% intensity for 14 minutes and 5 cm distance from the UV emission head. After cross-linking, the prints were placed in a 6-well cell culture plate (Sigma Aldrich), covered

with 2 ml McCoy culture medium, and incubated for six hours at 37°C.

**Cell viability post-printing-live/dead staining:** After six hours of incubation, the three bio printed samples were prepared for fluorescence imaging by a live dead staining-cell viability imaging kit (blue/green) purchased from (Invitrogen Thermo Fisher Scientific). The blue-green stain was added two drops/ml, and the samples were incubated for another 30 minutes at 37°C. They were then examined by Fluorescence Confocal Microscopy (DMI8, Leica, Germany) to compare the three samples in the ratio of living cells post-printing.

## Results and Discussion

In this section, the results will be exhibited in relation to the effect of the geometrical composition on cell viability. Thus, all the results aim to exhibit standardized conditions of SaOs-2 cells activity, GelMA biocompatibility, and printing procedures to prove that any differentiation in the cell viability between the three printed samples is only due to their geometrical composition “form physiology.” Since form physiology is closely dependent on its shape fidelity and high printing resolution. These aspects will also be discussed in terms of the printing fidelity of GelMA hydrogel, the effect of cells on rheological properties affecting their in-printing and post-printing fidelity as well as the 3D extrusion printing technique effect on cell viability, shape fidelity, and the geometrical design limitations. Thus, the results and discussion will be structured following this order: 3D extrusion bio printing effect on shape fidelity and cell viability; embedded cells effect on the rheological properties of the bionic; Saos-2 cells viability; GelMA biocompatibility and rheological properties; Geometrical Design effect on the prints shape fidelity/ resolution and cell viability.

**3D extrusion bio printing effect on shape fidelity and cell viability:** Generally, bio fabrication is defined as “the automatic fabrication of structurally optimized bio-functional products, employing: living cells, bioactive molecules, biomaterials, or hybrid cell-material constructs, through bio printing or bio assembly and subsequent tissue maturation processes” [34,35]. Over the last decade, bio fabrication through bio printing has witnessed increased research interest, especially the extrusion bio printing technologies, for exploring the possibility of one-pot printing procedures and printing micro-texture scale with resolutions reaching 10 µm scales. This ability to achieve micro scale resolution while maintaining rapid fabrication measured by the ratio of “Resolution/Time of Manufacturing (RTM)” is advantageous for various tissue engineering applications [36,34]. For example, by using these techniques, it is possible to bio-fabricate patient-customized constructs or implants that fit the geometrically complex and irregular forms of the native tissue through designing their complex forms using advanced digital design platforms or analyzing medical images. Moreover, micro-textured structures with adjustable pore networks can be optimized in terms of pore size and interconnectivity to facilitate nutrient circulation and consequently sustaining the encapsulated cells within the bio-fabricated tissue [37]. This potential has provoked the scaling of 3D extrusion bio printing technologies to a wider range of material development-based industries and architectural building materials, as is our case in the present work scope.

In 3D extrusion bio printing, a designed geometry is printed in a layer-by-layer fashion, as the bionic is extruded from the printer nozzle. This process is usually followed by a crosslinking procedure to

sustain the printed form [34]. Thus, extrusion bio printing techniques use hydrogels as building blocks, which limits the potential of creating more sophisticated, convoluted geometries, especially when printing ruled surfaces or out-of-plane features that are not aligned along a single plane when printing following Cartesian coordinates [38,39]. Despite these difficulties in achieving geometrical precision and shape fidelity by extrusion 3D printing, controlling the resolution of the 3D extruded printed structures remains an essential criterion for achieving biologically functional tissues. Proving the physiological dependence of formal geometrical fidelity. Thus, the prints must match the original digital designs. Nevertheless, optimizing bionics for bio printing involves multiple environmental stimuli and forces affecting the printing process and consequently the viability and activity of the encapsulated cells. Thus, imposing additional level of complexity for bio printing with living cells in comparison to the use of conventional biomaterial printing techniques [40].

**Embedded cells effect on rheological properties of the bio ink:** Since bio inks are aqueous-based hydrogels encapsulating living cells, they provide the embedded cells with a niche to thrive. Thus, these hydrogels are typically of low elastic modulus and biocompatible biochemical composition [37]. This, in turn, limits the micro printing resolution especially when printing in range of hundred micrometers to millimeters. These hydrogels also should maintain minimized shear stresses at the dispenser tip that is inversely correlated with the nozzle diameter to avoid damaging the embedded cells while printing [41]. While the viability of the embedded cells within a bio ink is an important aspect, they inversely affect the physicochemical properties of the ink as well, due to their occupancy of a specific volume distributed within the ink, according to their size, density, and aggregation. The volume occupied by the cells within the hydrogel hinders its cross-linking efficiency and viscoelastic properties. These encapsulated cells perform as a physical interference between different regions of the ink, hence limiting the bonding between reacting groups. For example, it was reported that the presence of cells ( $2.5 \times 10^6$  cells/mL) resulted in a decreased viscosity by 4-fold of gelatin methacryloyl bio ink compared to cell-free ink [42]. On the other hand, the encapsulated cells turn the bio ink into a composite material, behaving as colloidal systems exhibiting shear-thinning and increasing printability, especially with high densities of cell suspensions, even in the absence of rheological enhancers or additional biomaterials [43]. The effect of the cells on the viscoelastic properties of the bio ink is further complicated when cells are enclosed in a per cellular matrix, altering their mechanical properties [44], hydrodynamic radius, and boundary conditions at the fluid interface. Thus, resulting in irregular alterations of the bio ink rheological properties.

It was also reported that the embedded cells might actively interfere with the chemical processes driving the cross-linking reactions. For example, cells might capture free radicals generated from photo initiators or internalize small molecules, making them unavailable for chemical cross-linking [45].

The effects mentioned above of the embedded cells on the rheological properties, printing resolution, and cross-linking are also dependent on the metabolic state of the embedded cells, their subtype, encapsulation density, and occupied volume.

**Saos-2 cells viability:** In the current study, the authors used the Osteosarcoma SaOs-2 cell line due to their availability and reliable reproducibility in unlimited numbers without the need for isolation or ethical approval. Immortalized cell lines are easy to maintain and unlimitedly reproducible. The human osteosarcoma cell line SaOs-2 is

a phenotypically mature osteoblast with high levels of ALP activity, exceeding other osteosarcoma cell lines, such as MG-63 and SaOs-1 [46], that is in service of synthesizing autonomous bio mineralized materials with greater spatial dimensions and viability. Additionally, it was reported that the ALP activity by the SaOs-2 cell line was similar to human primary osteoblasts at the early time points but achieved 120-fold higher after 14 days of culturing under the same conditions [47]. It was reported also the capacity of SaOs-2 cells to form a calcified matrix typical of woven bone [48]. As well as, the high detailed similarity between the collagen structure synthesized by SaOs-2 and the collagen formed by primary human osteoblast cells but with a higher level of lysyl hydroxylation in the SaOs-2 cells [49]. Finally, the similarity between the cytokine and growth factor expression of SaOs-2 cells and primary normal human osteoblast cells [50,51]. These reported characteristics of the SaOs-2 cell line are congruent with the results reached in the current work. The SaOs-2 cells were employed in the current work due to their strong similarity to human isolated osteoblasts, giving the possibility of application on a wide spatial and volumetric scale due to its enhanced ability of proliferation. This was proven after only 14 days of incubation, achieving an  $8 \times 10^6$  cell count/T25 flask using the Neuberger chamber (Figure 3).

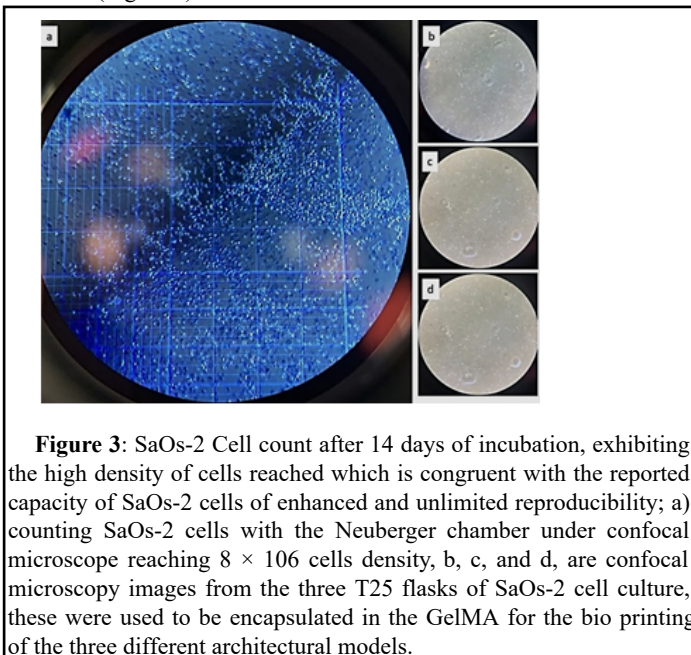


**Figure 3:** SaOs-2 Cell count after 14 days of incubation, exhibiting the high density of cells reached which is congruent with the reported capacity of SaOs-2 cells of enhanced and unlimited reproducibility; a) counting SaOs-2 cells with the Neuberger chamber under confocal microscope reaching  $8 \times 10^6$  cells density, b, c, and d, are confocal microscopy images from the three T25 flasks of SaOs-2 cell culture, these were used to be encapsulated in the GelMA for the bio printing of the three different architectural models.

Neuberger chamber under confocal microscope reaching  $8 \times 10^6$  cells density, b, c, and d, are confocal microscopy images from the three T25 flasks of SaOs-2 cell culture, these were used to be encapsulated in the GelMA for the bio printing of the three different architectural models.

Although numerous literatures have examined the activity of SaOs-2 cells with different bio ink composition, and the majority proved the competence of this cell line in achieving high viability and Alkaline Phosphate activity rate, the reporting of the effect of SaOs-2 cells on the rheological properties of GelMA bio inks had not yet been clearly addressed. However, we neutralized this condition in the current work, as it is standard for the three different geometrical designs and the standardized, unified composition of GelMA hydrogel, the printing technique, and time. Thus, the effect of SaOs-2 cells on the bioink rheology in the three prints is unified.

However, previous studies exhibited the consistency of SaOs-2 cell viability and activity even when encapsulated in different compositions of GelMA. For example, Sawyer et al. 2016 reported the unified effect of SaOs-2 cells on the aggregate lacunae diameter and the occupied area of encapsulated cells within three different GelMA compositions. In the reported study, the aggregate lacunae area and diameter were similar in all scaffolds at each growth stage [52].

**GelMA biocompatibility and rheological properties:** Extrusion bio printing requires hydrogels with the capacity to be extruded through a small-sized nozzle and subsequently maintain their shape stability post-printing. Despite the fact that natural hydrogels, such as gelatin-based hydrogels, are widely used due to their structural similarities to the native ECM, and their inherent signaling molecules that enhance cell adhesion, these hydrogels' mechanical properties are generally weak. Due to reducing their viscosity during extrusion to prevent excessive shear stresses from damaging the cells during the printing process. Thus, they are significantly deformed during the printing process, which could impair their shape fidelity [37]. Thus, successful extrusion bio printing requires hydrogels that display both flow and shape-retention properties, in order to maintain minimal internal resistance when passing through the printing nozzle, while retaining these forces to resist distortion after being dispensed from the nozzle with immediate flow discontinuation and elastic shape retention. To achieve this change, a tunable hydrogel with a further curing process should be developed.

GelMA is a semi-synthetic hydrogel that maintains the capacity of inherent biological signaling of the gelatin molecule while providing further control of the gel's mechanical properties [53]. GelMA is derived from the reaction of gelatin with meth acrylic anhydride, resulting in modification of lysine and hydroxyl residues with meth acrylamide and methacrylate side groups. After this derivatization process, the gelatin molecule retains many of its characteristics as the thermo-reversible physical cross-linking, as well as its biocompatible properties based on integrin-binding sequences and metalloprotease digestion sites. Thus, GelMA offers a biocompatible aqueous environment for cells to support their adhesion, growth, and proliferation. Modifying Gelatin with methacrylate side groups allows the GelMA molecule to rapidly polymerize in the presence of UV light and a Photoinitiator (PI), resulting in covalent cross-linking through the creation of a methacrylate backbone [54]. Consequently, giving GelMA stability at physiological temperature and allowing the optimization of its mechanical properties. Giving a resultant transparent material, which is adequate for microscopic analysis as well?

Given these features of biocompatibility, degradability, and low cost of GelMA, it has been used broadly for 3D cell culture applications and tissue engineering [55]. However, the great heterogeneity in the GelMA properties, concentrations, and polymerization are limiting the scale-up applications of GelMA. Furthermore, the differentiation in obtained results by many researchers in developing GelMA is complicating its usage, as there is no standardized, systematic approach for the adaptation of GelMA to a given cell type and intended application.

The GelMA polymerization is affected by multiple parameters that shape the final hydrogel properties and, consequently, affecting the encapsulated-cell growth inside the gel. Thus, these parameters including bio ink rheology and printing technique should be optimized to enable higher degree of formal complexity, spatial control, and resolution within a 3D bio print. Generally, it was reported the low

viscosity and poor resolution of printed constructs in low concentrations of GelMA with the most commonly used extrusion-based bio printers [56]. To overcome this, the majority of the previous studies print with higher concentrations of GelMA with higher cross-linking density [57,42]. This in turn, hinders the cell viability and proliferation rate by the effect of the dense polymer network [39]. Many studies have proposed some strategies to solve the poor printability of GelMA: such as the method of Billiet, et al. that exploited the inherent thermo-reversible properties of GelMA and printed at temperatures lower than 37°C. Another strategy to achieve shape fidelity is to cool the printing platform, to provoke the natural sol-gel transition of GelMA [42]. The later was applied in the current study, by cooling the printing bed to 4°C, which enhanced the gelation of GelMA post-print and pre-crosslinking, enabling its shape retention and cohesion.

Another reported approach to optimize GelMA printability is the thermoplastic co-deposition or the mixing of hyaluronic acid into the bio ink [58]. Although this approach is popular among research groups employing various rheological modifiers such as gellan gum [59] and nanoparticles [60] for enhancing GelMA deposition, there is no consensus for which rheological modifier works best for GelMA bio printing, not to mention the added cost of using such modifiers that hinder the scaling up of the GelMA prints. The modifier may be selected based on its viscosity-enhancing properties or depending on the final application, for example, calcium phosphate for bone tissue engineering [39]. However, using modifiers and fillers can also affect the viability of cells. Therefore, in the current study, a GelMA modifier-free hydrogel approach was adopted to avoid the possible effects of various modifiers on hindering cell adhesion, spreading, and proliferation [61,62].

In the current study, the biocompatibility of the prepared GelMA for SaOs-2 cells was tested. The metabolic activity assay proved a similar metabolic activity of the SaOs-2 cells seeded within GelMA compared to the control group of GelMA in Tissue Culture Plastic (TCP). Figure 4 exhibits the metabolic activity results proving the biocompatibility of GelMA.

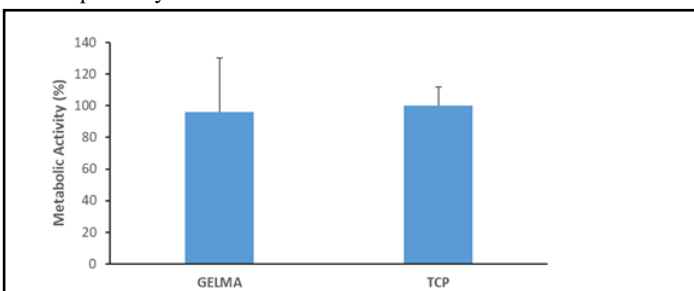


**Figure 4:** Metabolic Activity assay proving that SaOs-2 cells have a similar metabolic activity when seeded within GelMA in comparison to the tissue culture plastic (TCP).

Crosslinking is a typical process conducted to stabilize the extruded filaments, especially the most frequently applied photo induced cross-linking where photo initiators are added to the bio ink composition, and upon exposition to a certain range of light, they produce reactive species that trigger the polymerization process [63]. This process mainly employs ultraviolet A (UV-A) irradiation at wavelengths that do not cause significant DNA damage to the encapsulated cells [64]. Irgacure 2959 is one of the most commonly used photo initiators and photosensitizers used for GelMA cross-linking under UV exposure of

365 nm intensity. The photo-cross-linking in extrusion printing can be applied either in a layer-by-layer fashion or after completion of the entire print; the latter requires a better shape retention of the ink. In the current study, the cross-linking of GelMA was conducted by 365 nm UV exposure in the presence of the photoinitiator Irgacure 2959 for 14 minutes per layer to ensure maximum stability and shape fidelity of the prints [65]. Figure 5 shows the three prints of the three different digital designs after cross-linking.

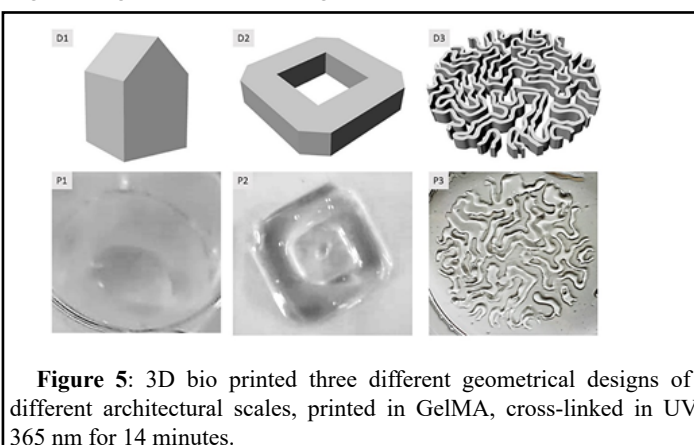


**Figure 5:** 3D bio printed three different geometrical designs of different architectural scales, printed in GelMA, cross-linked in UV 365 nm for 14 minutes.

**Geometrical Design effect on the prints' shape fidelity and cell viability:** Since hydrogels are the basic building blocks in extrusion bio printing, their geometrical design, planar orientation, and stacking during the layer-by-layer printing process are important parameters that influence both shape fidelity and cell viability. In the current study, the three designs experimented with three different approaches in geometrical form-finding and form making, with the aim of proposing developed material of living bone cells for feature application as a building material that is self-bio mineralized. The first design corresponded to a typical house with printing dimensions of (1 cm × 1 cm × 1.5 cm) of 1:1000 in architectural scale and extends over the multi-axial extensions, as it included the typical inclined roof of a conventional house. The second design corresponded to a typical Barcelona City building block with printing dimensions of (2 cm × 2 cm × 0.5 cm) of 1:5000 in architectural scale. It resembled an orthogonal design form based on direct extrusion of a chamfered square plan. The third design corresponded to a proposed urban design of Barcelona city with printing dimensions of (20 cm<sup>2</sup>) of 5 × 1010 in architectural scale, developed based on a form-finding simulation process that applied the differential growth algorithm. Originally, the differential growth model resembled the balance between the malignant osteosarcoma cells' infinite growth and the heterogeneous formation of normal bone tissue. As mentioned before, cells in developing bone tissue are exposed to multiple growth factors at various concentrations depending on cellular location, developmental stage, and nutrition. These affect the signaling pathways. In addition to these biochemical factors, cells in regenerating bone tissue experience a mechanical environment in which they are subject to forces through contact with neighboring cells and the extracellular matrix [66]. This mechanical stress over cells influences activity in bone formation, as they modulate their activity upon the mechanical feedback model. Since the osteocytes act as mechano-sensors through their network capacity to detect mechanical pressures and loads, they facilitate the adaptation of bone tissue to daily mechanical forces through regulation of osteoblast and osteoclast activities. Thus, the shape and spatial arrangement of the osteocytes are congruent with their sensing and signal transport functions, translating various mechanical stimuli

into biochemical signals. When coupling this mechanical feedback-derived bone tissue formation with the malignant growth and proliferation of the Osteosarcoma SaOs-2 cells used in this research for achieving increased spatial dimensions while preserving the formal physiological characteristics of bone tissue, the differential growth model is the congruent logic to achieve this balance by local tissue compression as faster-growing cells push against surrounding slower-growing cells. This compression controls the growth rate and distribution, restoring an even growth rate and reducing further compression and tissue distortion. Thus, in normal bone tissue, the mechanical feedback is a negative feedback that limits the extent to which a population of cells can overgrow [67]. This hypothesis that growth-induced compression controls growth rates, along with the observation that cells are more tightly packed at later stages of development, is presented in the current work in the differential growth algorithmic proposal for the Barcelona City urban design being one of the densest cities in Europe as the maximum major scale of future application of the developed GelMA-SaOs material while being in alignment with the physiological and formal characteristics of bone tissue formation to develop this bioactive building material for this urban design.

The differential growth model leads to the accumulation of mechanical stress within tissues. This mechanical stress results in reduced tension within faster-growing cells. This reduced tension increases the activity of the signaling pathway, which influences patterns of cell proliferation *in vivo*. Pan, et al. 2016 reported the mechanical feedback to describe the relationship between growth rates and tissue mechanics [66]. Therefore, this pattern sufficiently addresses the increasing population density that occupy a limited space, with the micro-texture tuning effect congruent with the stress (the density) applied to the structures. However, in the current study, this micro-texture tuning effect is not experimented complying with the main objective to prove the effect of the general geometry composition on cell viability. Nevertheless, ongoing research is being conducted to enhance the printability of GelMA with various fillers to enable its 3D bio printing on a micro-texture scale to achieve optimized shape fidelity and cell viability.

As shown in Figure 5, the bio ink composition, cell count, printing settings, and cross-linking were all standardized in the three geometrical designs. However, they exhibited significantly varied shape fidelity and resolution as well as varied cell viability.

The ability to extrude a uniform linear filament is affected by the printing pressure and the nozzle speed, as well as the nozzle offset [56,68,69]. In the current study, the nozzle offset was reduced to 0.01 cm to avoid swelling. The printing speed was customized to 100% to reduce the printing time to maintain cell viability. In the three prints, the printing files were adjusted to rectangular grid infill to achieve high shape fidelity, as reported for structures with transversal porosity to prevent filament collapse along the axial direction due to the effect of gravity, especially when a filament is spanning over a large span. It was previously reported that the maximum gravity-defying gap sizes range between 1-12 mm [70,71], minimizing the angle of deflection as the function of the gap distance, measuring the deformation suffered by the bio ink due to the discrepancy between the gravitational force given by the bio ink's own weight, and inertia measured by yield stress and storage modulus of the ink [70]. These parameters, along with the nozzle diameter of 0.3 and geometrical composition, greatly affected the final resolution of the prints. In the current study, Figure 5. Shows the generally low resolution of the prints corresponding to

the three designs. However, the second design of the Barcelona Block was the best geometry to achieve coherency and shape fidelity in comparison to the two other designs and, in comparison, to the original 3D digital designs. This is due to its orthogonal plane and the unified axial extrusion method applied in its form, making it congruent with its printing settings.

Printing planar forms depends mainly on filament homogeneity and uniformity since planar structures extend along two directions *x* and *y* planes and are significantly wider than the height of the construct [72,73]. The fusion between layers causes the increase in diameter in the *x-y* plane, as the filament relaxes and spreads onto the underlying layer [74,75]. This type of structures enables the evaluation of the geometrical accuracy of GelMA prints and their match with the original digital design model. As measuring the filament width (*x-y* plane) and thickness (*z*-axis) across multiple points along the length of the planar structure was compared to the original dimensions of the digital design created with Rhinoceros 3D at the same points [72].

The differential growth pattern still showed high similarity to the original 3D digital design. However, this print exhibited swelling and infusion of distanced lines in comparison to the original digital design. This could be justified due to the confined dimension of each singular line only being 0.3 cm in width, the non-uniform interspatial dimension between each line, and the neighboring lines, which also had 0.3-0.5 margins, and the spatial extension over a wide area of the general deferential growth form. This results in partial layer collapse or swelling effect of the earlier printed zones. Concurrently, the later zones were still in printing before they all under grow the UV cross-linking. Thus, and as it was reported previously, the adjacent filaments printed in the same layer are prone to fuse due to the time-dependent flow prior to stabilization *via* cross-linking and spreading onto the underlying layer caused by surface tension [70]. In such a meandering pattern, the fused portion of the filament propagates from the corner and increases to cause a complete fusion of the filaments, closing the intraligamentary space. Thus, this geometrical composition requires increased bio ink viscosity, which could affect cell viability, or requires the customization of the digital design printing file, to section the printing process by subsequent zones, giving time margins for UV cross-linking between each zone. Despite that, the latter sounds plausible. However, this will increase the total printing time of the design and consequently affect the cell viability and the ink viscosity being exposed to printing temperature and stress of the printing head. Thus, this aspect requires further investigation and manipulation of the printing settings.

The slow stabilization of the ink after dispensing and pre-crosslinking and fusion of adjacent filaments causes the collapse of the filament circularity [76,77]. The literature reported that the ideal axial porosity is in a 0-90° laydown pattern that displays a square or rectangle, according to the designed strand-to-strand distances, in the *x-y* plane. This proposes that high geometric accuracy would result in a printability index of  $Pr=1$  (square shape transversal pore geometry). However,  $Pr<1$  and  $Pr>1$  correspond to a more round or irregularly shaped transversal geometry, respectively [78,79]. Low viscosity and no optimal gelation conditions are some of the causes for these deviations, resulting in the merging of filaments and the resulting low shape fidelity [80]. These parameters contributed to hindering the shape fidelity of the differential growth pattern design. Thus, the current study conducted approaches, such as post-printing UV cross-linking, to increase filament stability after extrusion [81].

The conventional house design print failed to exhibit any relevance to its original 3D digital design, with reduced resolution. This was caused by the incongruence between the digital form-making method used to build the model and the layering method for the printing process. This design is a multi-axial design that exhibits inclined surfaces in different axes. Thus, to print this form, it was adjusted to a planer configuration so that the inclined pointy ends of the form are in a planer position to avoid the collapse of the higher layers of these inclined surfaces. However, the moderate to low viscosity of GelMA failed to deliver this pointy inclined surface with high resolution. Thus, it could be concluded that multiracial designs require high-viscosity gels to deliver sufficiently high-resolution printing.

These shape fidelity evaluations per printed design were done using real-time monitoring through a built-in HD camera Tool head in the Bio X printer. However, future proposed micro-texture sophisticated prints require more accurate tools to evaluate the levels of deviations between the final prints and the original digital designs. One of these tools is 3D Computed Tomography (CT) imaging, where constructs can be visualized by CT [72] using decreased beam intensity and focusing on the lower range of the gray values [82]. Another feasible method is Optical Coherence Tomography (OCT) that allows 3D visualization of water-rich samples, such as hydrogels, providing a 3D volumetric view of the inner microstructure of a translucent construct [83,84]. This allows real-time quantitative assessment of morphological parameters, including pore size, filament size, porosity, surface area, and pore volume with high contrast between hydrogel and pores with high resolution (1-10  $\mu\text{m}$ ) [72]. Moreover, OCT imaging overweighs fluorescence or scanning laser confocal microscopy, thanks to the increased penetration depth of up to 1000  $\mu\text{m}$ , while fluorescence microscopy only allows the analysis of the construct surface, and the penetration depth of confocal microscopy is limited to 300  $\mu\text{m}$  [85]. Furthermore, OCT is noninvasive and uses only a low exposure dose [72], and, the outcome can be directly compared with the original digital design file, thus, providing real-time feedback for optimizing shape fidelity of the printed designs.

The aforementioned effect of GelMA on the deformation of the printed 3D constructs and their deviation from the original digital design, requires the development of extrusion printing technologies and strategies to further tune all the related previously mentioned parameters. The majority of these parameters are directly related with the physicochemical properties of the bio ink. Among the most common methods is refining the bio ink's design so that its rheological behavior and properties can prevent or minimize such deformations. This approach includes adding rheological modifiers and viscosity enhancers in the form of micro and nanoparticles [86], Nano fibrous elements [87], Nano clay [88], or blends of different biomaterials [89]. While these methods propose a direct modification of the ink's chemical composition or physical form, other approaches focus at modifying the surrounding environment and the printing process conditions or the printing hardware to optimize the timing in which stabilization and cross-linking occur within an ink. These approaches would enable the exploitation of biocompatible bio inks that provide biomimetic environment for cells to thrive, while overcoming their poor printability when using the conventional methods.

Given the geometrical design effect on shape fidelity, it was necessary to relate the obtained results with this geometrical design effect on cell viability as well, being the main objective of the study. The live/dead staining revealed a general decrease in cell viability among the three different prints. However, the second design of the

Barcelona Building Block achieved the highest cell viability in comparison to the two other prints (Figure 6).

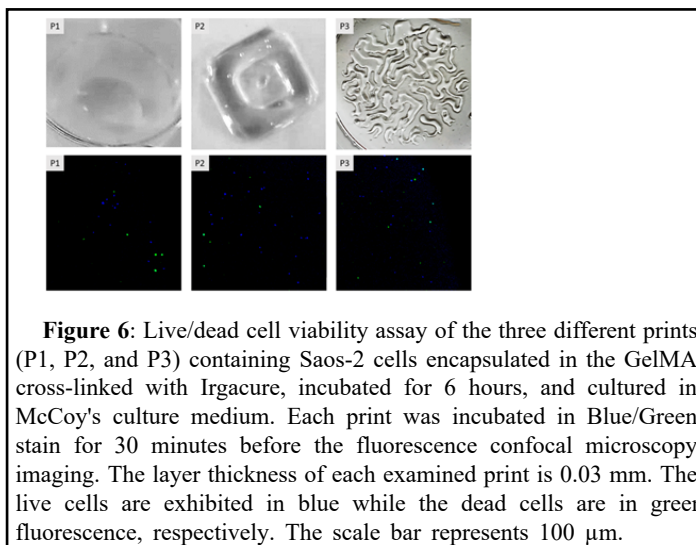


**Figure 6:** Live/dead cell viability assay of the three different prints (P1, P2, and P3) containing Saos-2 cells encapsulated in the GelMA cross-linked with Irgacure, incubated for 6 hours, and cultured in McCoy's culture medium. Each print was incubated in Blue/Green stain for 30 minutes before the fluorescence confocal microscopy imaging. The layer thickness of each examined print is 0.03 mm. The live cells are exhibited in blue while the dead cells are in green fluorescence, respectively. The scale bar represents 100  $\mu\text{m}$ .

The results obtained from the confocal fluorescence microscopy revealed the congruency between the highest shape fidelity and the highest cell viability achieved by the second geometrical design of the Barcelona Block, followed by the differential growth geometry, and lastly, the conventional house design, which corresponds typically with the shape fidelity of each of these designs. These results revealed that the orthogonal square or rectangular planar form with microtexture of a rectangular grid is the most biocompatible and maintains an adequate circulation of media and oxygen to attain cell viability.

This could be further justified by considering different aspects that affect cell viability in the printed bio ink. In vivo, cells exist within a complex and dynamic microenvironment that offers structural support for cells, while encompassing various biochemical interactions at cell adhesion sites, and biophysical interactions such as topography, porosity, and rigidity signals that together control the cell behavior, in terms of cell spreading, migration, differentiation, and self-renewal [90].

As mentioned previously, in vivo, the network of febrile proteins and polysaccharides which compose the ECM, anchors the cells within their specific microenvironment. This mechanical relation between the cells and the ECM occurs through Tran's membrane proteins or integrin's [91] that bind specific cell-adhesive ligands offered by ECM proteins, connecting the ECM to the intracellular actin cytoskeleton. During cell spreading and growth, the ECM could undergo mechanical deformation and remodeling by the cells [92]. On the other hand, the mechanical properties of the ECM alter the ability of cells to generate tension, modulate cell spreading, control nuclear shape, and regulate the intercellular signaling pathways. These mechanical properties that influence cell behavior include bulk stiffness, local stiffness, strain-stiffening, and stress-relaxation [90].

As much as these parameters depend on the use of hydrogel rheology in the first place, they depend on the geometrical design in an interconnected translation between these mechanical forces and their geometrical cues. For example, the substrate stiffness characterized by the elastic or Young's modulus of the hydrogel imposes resistance to the cells that can sense this resistance and regulate their spreading and proliferation rate. This occurs through the

Mechano-transduction process, where a mechanical stimulus, such as stretching, shear stress, or substrate rigidity, is converted into chemical signals that control cell fate [93]. Through focal adhesions [94], cell-cell interactions, Mechano-sensors [93], and nuclear signaling elements [95], which together act to modify protein and gene expression profiles. It was reported that substrates with stiffness's ranging from a few hundred Pa to MPa have been prepared as hydrogels, including natural materials such as gelatin and alginate, to culture cells. Cells cultured on these hydrogels showed responsiveness to the degree of stiffness by altering their adhesion, spreading, morphology, and migration characteristics [96]. Cell spreading is also affected by stiffness [97], as it was reported by Yang et al. that hMSCs cultured on hydrogels with higher concentrations of stiff regions showed more spread, elongated cell morphologies, and higher osteoblast differentiation [98], indicating that local variations in the underlying substrate mechanical properties might regulate cell adhesion, spreading, and nuclear transcription effectors [95]. Furthermore, it was recently shown that stiffer substrates give rise to nuclear flattening, stretching nuclear pores and reducing their mechanical resistance to molecular transport [99]. In addition, when subjected to a stiffness gradient, cells display directed migration toward stiffer regions [100]. However, unlike bulk stiffness, where increased stiffness promotes cell spreading, materials with soft local stiffness have greater flexibility in changing their conformations to optimize cell contact and thereby trigger cell spreading. If the fiber stiffness is higher, the transfer of cellular traction forces to nearby fibers will be limited. Consequently, cells are unable to build up sufficient tension, which may suppress cell spreading and migration. On the other hand, normally, the fibrous nature of the ECM creates a unique microenvironment that enables long-range mechanical cell-cell communication *via* cell-induced remodeling of the network [101]. Thus, it was reported that increased local fiber stiffness can withstand the repetitive contractile pulling at cell adhesion sites, which reinforces the stability of cellular adhesion and maturation of cells [102]. Another parameter is the stress relaxation, which indicates the decrease of stress in response to the constant applied strain with increasing time [103]. Recently, numerous studies reported attempts to design hydrogels with tunable stress relaxation properties by changing the hydrogel composition or concentration [103], molecular weight [104], cross-link type or density [105], and degradation [106]. Those studies manifested the significant effect of stress relaxation on cell fate decisions. For example, reported that when hMSCs are encapsulated in 3D alginate hydrogels with faster relaxation properties, they show enhanced spreading, proliferation, and estrogenic differentiation.

Mechano-transduction signaling in a 3D environment is also dependent on other parameters such as dimensionality and degradability of the gel. For example, Khatami et al, 2013. Have proved that cell spreading was limited in hydrogels with a high density of no degradable cross-links. Another parameter that affects cell viability and migration in hydrogels is the influence of confinement, as cells migration behavior in confinement is typically straight [100], and migration speed is significantly higher in micro channels than on 2D substrates [107,108]. Fully confined cells display a sliding migration [109,110]. Geometric confinement also influences cell morphology [111]. Taken together, these studies clearly show that confinement which is typically dependent on the geometrical design of a print, gives rise to marked changes in the cellular cytoskeleton structure, cellular adhesion distributions, cell migration behavior, and morphology, indicating that cells are responsive to the physical confinement.

Another important parameter is the relation between the encapsulated cells' geometrical cues as size and shape, and the geometrical design of the print and how this affects cell fate regulation. Many studies reported the influence of these cues by culturing cells on micro patterned ECM islands of defined geometries, fabricated with various techniques, as micro contact printing/stamping, micro wells with different geometries, sizes, and cell printing. These studies [112] revealed that cells prefer to generate larger tension at curvature, partially because of the confinement [113]. Furthermore, the molecular mechanism of cell-geometry-dependent regulation of morphological differentiation has been elucidated in some cases [114]. A recent study suggested that cell geometry regulates cell signaling *via* modulation of plasma membrane order [115]. Studies on cell geometry have shown that cell fate can be guided between apoptosis, growth, and differentiation by altering the extent to which the cell can physically expand and flatten [116,117]. It has been shown that confining cells on patterned surfaces could significantly alter the structural organization of the nuclear lamina compared with cells on flat surfaces [118]. Substrate topographies such as grooves, steps, pits, etc., also strongly control cell shape and lineage selection. For example, Desai et al. fabricated a substrate with spatially organized multiple adhesive ligands patterns. They found that cells can sense surface geometry by segregating single integrin's on the surface of cells to regulate ECM-specific binding [119]. Moreover, when scaling these studies to the level of complex tissues, tissue in sharp corners (for example, triangular channel) was thicker than those in square and hexagonal channels, following the decrease of local curvature and indicating that increasing local curvature can increase the rate of proliferation [120].

Furthermore, numerous recent studies have also shown that geometrical cues affect the orientation of cell motility, as well [121], as the polarity axes as defined by the internal and cortical cell asymmetry were controlled by the adhesive geometry [122], when cells were cultured on ECM islands with square or rectangle geometry [123]. The cell shape within tissue can reflect the past physical and chemical signals that the cells have run into. The cellular phenotype can also be controlled by the cell shape information, as shown in Ron et al. study that used micro fabricated 3D biomimetic chips to demonstrate that 3D cell shape can control cell phenotype *via* cell tension [124].

However, the study of the geometrical design effect on cell proliferation, migration, function, and morphology requires further investigation to assess the influence of geometrical control after long-term culture when the cells produce their own ECM and loose direct links with micro scale or nanoscale geometrical cues, as well as, investigating the feasibility of applying findings on 2D substrates to 3D, and most importantly, the underlying molecular mechanisms by which cells sense and respond to the geometric cues. The 3D microenvironment provides the cells with a polarized environment to grow and form adhesive connections on all sides. The 2D polarized environment leads to asymmetric distribution of cell adhesions and corresponding alterations in cell functions. Besides, unlike cell spreading and adhesion on a 2D substrate that is unlimited without any physical limits, the bounding surrounding matrix significantly hinders the fully embedded cells from spreading and migrating, obligating cells to penetrate the matrix pores or degrade the matrix around them before spreading and migration becomes possible. Moreover, on 2D substrates, the speed of migration is determined by the actin polymerization, integrin-mediated adhesion, and myosin-mediated cellular contraction. In a 3D matrix, the contribution effectors to cell

migration are more complex, involving local ECM stiffness [102], membrane degradation [125,126], and microtubule dynamics [125]. Consequently, the speed of cell migration and its response to stiffness differs between 2D compared to 3D. Furthermore, on 2D substrates, cell culture medium, soluble factor, and cell-secreted factors can undergo free diffusion. However, in 3D matrices, diffusion of oxygen, proteins, and small molecules can be limited, resulting in gradients [90].

Further study is needed to understand how cells accumulate information about their environmental geometrical properties over time, how external physical stimuli are translated molecularly into cell fate decisions, and how these decisions manifest themselves in changes in cell phenotype [127].

## Conclusion

The current study aimed to propose the use of GelMA-based bionic, direct extrusion bio printing, and osteosarcoma cells to develop a self-bio mineralized material that can be applied as an architectural building material in the future. The main criteria for such material are extended spatial dimensions, high shape fidelity, and resolution. In relevance to this aim, the main question of the current work was to examine the effect of geometrical composition on cell viability and shape fidelity, these being the two main attributes for achieving the bio mineralized building material. The experimental procedures conducted were in agreement to standardize all the parameters that could affect cell viability in the 3D direct extrusion bio printing process. Starting from the GelMA hydrogel composition, cross-linking, SaOs-2 cells culturing, cells encapsulation, and printing settings. The hypothesis was tested through three different geometrical designs, each corresponding to a different architectural scale from the house to the city. The results revealed that the most potent geometrical design to achieve shape fidelity, cell viability, and spreading was generated from a square orthogonal plan with a rectangular grid for infill, followed by a differential growth form that was generated from a form-finding simulation of the differential growth algorithm based on the interpretation of the balance between unlimited growth and proliferation of SaOs-2 cells and the bio mineralized bone tissue structure in vivo. The results also revealed the significant influence of the hydrogel rheological properties, especially the viscosity, on the shape fidelity of the final prints while exhibiting high biocompatibility rates. Thus, further study is needed to enhance GelMA rheological properties to enable the high-resolution printing of more complex geometrical forms while maintaining the same high biocompatibility rates. It is also recommended to have further optimization and customization of complex geometrical forms in terms of micro-structures to attain high shape fidelity post-printing while maintaining high cell viability rates.

## References

1. Kriegman S, Blackiston D, Levin M, Bongard J (2020) A scalable pipeline for designing reconfigurable organisms. *PNAS* 117(4): 1853-1859.
2. Estevez AT (2014) The Future of Architecture: Biodigital Architecture and Genetics. *Arch Res* 4(1B):13-20, Scientific & Academic Publishing Co., Rosemead-California.
3. Robling AG, Castillo AB, Turner CH (2006) Biomechanical and molecular regulation of bone remodeling. *Annu Rev Biomed Eng* 8(1): 455-498.
4. Buckwalter JA, Glimcher MJ, Cooper RR, Recker R (1995) Bone Biology. *J Bone Joint Surg* 77(8): 1276-1289.
5. Clarke B (2008) Normal Bone Anatomy and Physiology. *Clin J Am Soc Nephrol*: S131-S139.
6. Sims NA, Gooi JH (2008) Bone remodeling: Multiple cellular interactions required for coupling of bone formation and resorption. *Semin Cell Dev Biol* 19(5): 444-451.
7. Florencio-Silva R, Sasso GR da S, Sasso-Cerri E, Simoes MJ, Cerri PS, et al. (2015) Biology of Bone Tissue: Structure, Function, and Factors That Influence Bone Cells. *BioMed Research International*. 1-17.
8. Dallas SL, Prideaux M, Bonewald LF (2013) The Osteocyte: An Endocrine Cell and More. *Endocr Rev* 34(5): 658-690.
9. Khosla S, Oursler, MJ Monroe DG (2012) Estrogen and the skeleton. *Trends Endocrinol Metab* 23(11): 576-581.
10. Raisz LG, Rodan GA (1998) Embryology and cellular biology of bone, in *Metabolic Bone Disease and Clinically Related Disorders*, L V Avioli and S M Krane, eds, 1-22, Academic Press, New York, 3rd edition.
11. Baht GS, Hunter GK, Goldberg HA (2008) Bone sialoprotein-collagen interaction promotes hydroxyapatite nucleation. *Matrix Biol* 27: 600-608.
12. Lin S, Cao L, Wang Q, Du J, Jiao D, et al (2018) Tailored biomimetic hydrogel based on a photopolymerised DMP1/MCF/gelatin hybrid system for calvarial bone regeneration. *J Mater Chem* 6(3): 414-427.
13. Yu Y, Wang L, Yu J, Lei G, Yan M, et al. (2014) Dentin matrix proteins (DMPs) enhance differentiation of BMMSCs via ERK and P38 MAPK pathways. *Cell Tissue Res* 356(1): 171-182.
14. White KA, Cali VJ, Olabisi RM (2021) Micropatterning biomineralization with immobilized mother of pearl proteins. *Sci Rep* 11(1):2141.
15. White KA, Olabisi RM (2019) Spatiotemporal control strategies for bone formation through tissue engineering and regenerative medicine approaches. *Adv Healthc Mater* 8: 1801044.
16. Liu HW, Chen CH, Tsai CL, Lin IH, Hsiue GH, et al. (2007) Heterobifunctional poly(ethylene glycol)-tethered bone morphogenetic protein-2-stimulated bone marrow mesenchymal stromal cell differentiation and osteogenesis. *Tissue Eng* 13: 1113-1124.
17. He X, Ma J, Jabbari E (2008) Effect of grafting RGD and BMP-2 protein-derived peptides to a hydrogel substrate on osteogenic differentiation of marrow stromal cells. *Langmuir* 24: 12508-12516.
18. Capulli M, Paone R, Rucci N (2014) Osteoblast and osteocyte: Games without frontiers. *Arch Biochem Biophys* 561: 3-12.
19. Marks SC, Popoff S N (1988) Bone cell biology: The regulation of development, structure, and function in the skeleton. *J Anat* 183(1): 1-44.
20. Grigoriadis AE, Heersche JN, Aubin JE (1988) Differentiation of muscle, fat, cartilage, and bone from progenitor cells present in a bone-derived clonal cell population: effect of dexamethasone. *J Cell Biol* 106(6): 2139-2151.
21. Ducy P, Zhang R, Geoffroy V, Ridall AL, Karsenty G (1997) *Osf2/Cbfa1*: A Transcriptional Activator of Osteoblast Differentiation. *Cell* 89(5): 747-754.
22. Kapinas K, Kessler C, Ricks T, Gronowicz G, Delany AM (2010) miR-29 Modulates Wnt Signaling in Human Osteoblasts

- through a Positive Feedback Loop. *J Biol Chem* 285(33): 25221-25231.
23. Anderson HC (2003) Matrix vesicles and calcification. *Curr Rheumatol Rep* 5(3): 222-226.
24. Yoshiko Y, Candeliere GA, Maeda N, Aubin JE (2007) Osteoblast Autonomous P i Regulation via Pit1 Plays a Role in Bone Mineralization. *Mol Cell Biol* 27(12): 4465-4474.
25. Glimcher MJ (1998) "The nature of the mineral phase in bone", in *Metabolic Bone Disease*, MJ Glimcher, ed. 23-50, Academic Press, San Diego.
26. Boivin G, Meunier PJ (2002) The Degree of Mineralization of Bone Tissue Measured by Computerized Quantitative Contact Microradiography. *Calcif Tissue Int* 70(6): 503-511.
27. Franz-Odenaal TA, Hall BK, Witten PE (2005) Buried alive: How osteoblasts become osteocytes. *Developmental Dynamics* 235(1): 176-190.
28. Structural Materials. (2012). TheFreeDictionary.com.
29. Clark J (2019) Metallic Bonding Retrieved from Chemistry LibreTexts.
30. Aamodt JM, Grainger DW (2016) Extracellular matrix-based biomaterial scaffolds and the host response. *Biomaterials* 86: 68–82.
31. Chen Y, Feng Y, Deveaux J G, Masoud M, Chandra FS, et al. (2019) Biomineralization Forming Process and Bio-inspired Nanomaterials for Biomedical Application: A Review *Minerals* 9: 68.
32. Bosch-Rue, E, Diez-Tercero L, Giordano-Kelhoffer B, Delgado LM, Bosch BM, et al. (2021) Biological Roles and Delivery Strategies for Ions to Promote Osteogenic Induction. *Front Cell Dev Biol* 8.
33. Nguyen AK, Goering PL, Reipa V, Narayan RJ (2019) Toxicity and photosensitizing assessment of gelatin methacryloyl-based hydrogels photoinitiated with lithium phenyl-2,4,6-trimethylbenzoylphosphinate in human primary renal proximal tubule epithelial cells. *Biointerphases* 14(2): 021007.
34. Moroni L, Boland T, Burdick JA, De Maria C, Derby B, et al. (2018) Biofabrication: A Guide to Technology and Terminology. *Trends Biotechnol* 36(4): 384-402.
35. Groll J, Boland T, Blunk T, Burdick JA, Cho DW, et al. (2016) Biofabrication: reappraising the definition of an evolving field. *Biofabrication* 8(1): 013001.
36. Lee A, Hudson AR, Shiwarski DJ, Tashman JW, Hinton TJ, et al. (2019) 3d Bioprinting of Collagen to Rebuild Components of the Human. *Heart Science* 365: 482-487.
37. Schwab A, Levato R, D'Este M, Piluso S, Eglin D, et al. (2020) Printability and Shape Fidelity of Bioinks, in *3D Bioprinting*. *Chem Rev* 120(19): 11028-11055.
38. De Ruijter M, Hrynevich A, Haigh JN, Hochleitner G, Castilho M, et al. (2017) Out-of-Plane 3D-Printed Microfibers Improve the Shear Properties of Hydrogel Composites. *Small* 14(8): 1702773.
39. Malda J, Visser J, Melchels FP, Jungst T, Hennink WE, et al. (2013) 25th Anniversary Article: Engineering Hydrogels for Biofabrication. *Advanced Materials* 25(36): 5011-5028.
40. Datta, P, Vyas V, Dhara S, Chowdhury AR, Barui A (2019) Anisotropy Properties of Tissues: A Basis for Fabrication of Biomimetic Anisotropic Scaffolds for Tissue Engineering. *J Bionic Eng* 16(5): 842-868.
41. Müller M, Ozturk E, Arlov O, Gatenholm P, Zenobi-Wong M (2016) Alginate Sulfate-Nanocellulose Bioinks for Cartilage Bioprinting Applications. *Ann Biomed Eng* 45(1): 210-223.
42. Billiet T, Gevaert E, De Schryver T, Cornelissen M, Dubruel P (2014) The 3D printing of gelatin methacrylamide cell-laden tissue-engineered constructs with high cell viability. *Biomaterials* 35(1): 49-62.
43. Jeon O, Lee YB, Jeong H, Lee SJ, Wells D, et al. (2019) Individual cell-only bioink and photocurable supporting medium for 3D printing and generation of engineered tissues with complex geometries. *Materials Horizons* 6(8): 1625-1631.
44. Guilak F, Alexopoulos LG, Haider MA, Ting-Beall HP, Setton LA (2005) Zonal Uniformity in Mechanical Properties of the Chondrocyte Pericellular Matrix: Micropipette Aspiration of Canine Chondrons Isolated by Cartilage Homogenization. *Ann Biomed Eng* 33(10): 1312-1318.
45. Petta D, Armiento AR, Grijpma D, Alini M (2018) 3D bioprinting of a hyaluronan bioink through enzymatic-and visible light-crosslinking *Biofabrication* 10(4): 044104.
46. Murray E, Provvedini D, Curran D, Catherwood B, Sussman H, et al. (2009) Characterization of a human osteoblastic osteosarcoma cell line (SAOS-2) with high bone alkaline phosphatase activity. *JBMR* 2(3): 231-238.
47. Saldaña L, Bensiamar F, Bore A, Vilaboa N (2011) In search of representative models of human bone-forming cells for cytocompatibility studies. *Acta Biomaterialia* 7(12): 4210-4221.
48. Rodan SB, Imai Y, Thiede MA, Wesolowski G, Thompson D, et al. (1987) Characterization of a human osteosarcoma cell line (Saos-2) with osteoblastic properties. *Cancer Res* 47: 4961-4966.
49. Fernandes RJ, Harkey MA, Weis M, Askew JW, Eyre DR (2007) The post-translational phenotype of collagen synthesized by SAOS-2 osteosarcoma cells. *Bone* 40(5): 1343-1351.
50. Bilbe G, Roberts E, Birch M, Evans DB (1996) PCR phenotyping of cytokines, growth factors and their receptors and bone matrix proteins in human osteoblast-like cell lines. *Bone* 19(5): 437-445.
51. Czekanska EM, Stoddart MJ, Richards RG, Hayes JS (2012) In search of an osteoblast cell model for in vitro research. *Eur Cells Mater* 24: 1-17.
52. Sawyer SW, Oest ME (2016) Behavior of Encapsulated Saos-2 Cells within Gelatin Methacrylate Hydrogels. *J Tissue Eng* 7(2).
53. Ruedinger F, Lavrentieva A, Blume C, Pepelanova I, Schepel T (2014) Hydrogels for 3D mammalian cell culture: a starting guide for laboratory practice. *Appl Microbiol Biotechnol* 99(2): 623-636.
54. Yue K, Trujillo-de Santiago G, Alvarez MM, Tamayol A, Annabi N, et al. (2015) Synthesis, properties, and biomedical applications of gelatin methacryloyl (GelMA) hydrogels. *Biomaterials* 73: 254-271.
55. Loessner D, Meinert C, Kaemmerer E, Martine LC, Yue K, et al. (2016) Functionalization, preparation and use of cell-laden gelatin methacryloyl-based hydrogels as modular tissue culture platforms. *Nat Protoc* 11(4): 727-746.
56. Hölzl K, Lin S, Tytgat L, Van Vlierberghe S, Gu L, et al. (2016) Bioink properties before, during and after 3D bioprinting. *Biofabrication* 8(3): 032002.
57. Lee B, Lum N, Seow L, Lim P, Tan L (2016) Synthesis and Characterization of Types A and B Gelatin Methacryloyl for Bioink Applications. *Materials* 9(10): 797.

58. Schuurman W, Levett PA, Pot MW, Van Weeren PR, Dhert WJA, et al. (2013) Gelatin-Methacrylamide Hydrogels as Potential Biomaterials for Fabrication of Tissue-Engineered Cartilage Constructs. *Macromol Biosci* 13(5): 551-561.
59. Melchels FPW, Dhert WJA, Hutmacher DW, Malda J (2014) Development and characterisation of a new bioink for additive tissue manufacturing. *J Mater Chem B* 2(16): 2282.
60. Xavier JR, Thakur T, Desai P, Jaiswal MK, Sears N, et al. (2015) Bioactive Nanoengineered Hydrogels for Bone Tissue Engineering: A Growth-Factor-Free Approach. *ACS Nano* 9(3): 3109-3118.
61. Zhu M, Wang, Y, Ferracci G, Zheng J, Cho N-J, et al. (2019) Gelatin methacryloyl and its hydrogels with an exceptional degree of controllability and batch-to-batch consistency. *Sci Rep* 9(1): 1-13.
62. Nichol JW, Koshy ST, Bae H, Hwang CM, Yamanlar S, et al. (2010) Cell-laden microengineered gelatin methacrylate hydrogels. *Biomaterials* 31(21): 5536-5544.
63. Lim KS, Galarraga JH, Cui X, Lindberg GCJ, Burdick JA, et al. (2020) Fundamentals and Applications of Photo-Cross-Linking in Bioprinting. *Chem Rev* 120(19): 10662-10694.
64. Widel M, Krzywon A, Gajda K, Skonieczna M, Rzeszowska-Wolny J (2014) Induction of bystander effects by UVA, UVB, and UVC radiation in human fibroblasts and the implication of reactive oxygen species. *Free Radic Biol* 68: 278-287.
65. Fedorovich NE, Swennen I, Girones J, Moroni L, van Blitterswijk CA, et al. (2009) Evaluation of Photocrosslinked Lutrol Hydrogel for Tissue Printing Applications. *Biomacromolecules* 10(7): 1689-1696.
66. Pan Y, Heemskerck I, Ibar C, Shraiman BI, Irvine KD (2016) Differential growth triggers mechanical feedback that elevates Hippo signaling. *PNAS* 113(45): E6974-E6983.
67. Bi Y, Stuelten CH, Kilts T, Wadhwa S, Iozzo RV, et al. (2005) Extracellular Matrix Proteoglycans Control the Fate of Bone Marrow Stromal Cells. *Int J Biol Chem* 280(34): 30481-30489.
68. Gu Z, Gao Z, Liu W, Wen Y, Gu Q (2019) A Facile Method to Fabricate Anisotropic Extracellular Matrix with 3D Printing Topological Microfibers. *Materials* 12(23): 3944.
69. Sarker Md, Chen XB (2017) Modeling the Flow Behavior and Flow Rate of Medium Viscosity Alginate for Scaffold Fabrication with a Three-Dimensional Bioplotter. *J Manuf Sci Eng* 139(8).
70. Ribeiro A, Blokzijl MM, Levato R, Visser CW, Castilho M, et al. (2017) Assessing bioink shape fidelity to aid material development in 3D bioprinting. *Biofabrication* 10(1): 014102.
71. Therriault D, White SR, Lewis JA (2007) Rheological Behavior of Fugitive Organic Inks for Direct-Write Assembly. *Appl Rheol* 17(1): 10112-10118.
72. Wang L, Xu M, Luo L, Zhou Y, Si P (2018) Iterative feedback bio-printing-derived cell-laden hydrogel scaffolds with optimal geometrical fidelity and cellular controllability. *Sci Rep* 8(1).
73. Chung JHY, Naficy S, Yue Z, Kapsa R, Quigley, et al. (2013) Bio-ink properties and printability for extrusion printing living cells. *Biomater Sci* 1(7): 763-773.
74. Göhl J, Markstedt K, Mark A, Håkansson K, Gatenholm P, et al. (2018) Simulations of 3D bioprinting: predicting bioprintability of nanofibrillar inks. *Biofabrication* 10(3): 034105.
75. Ahn G, Min KH, Kim C, Lee J-S, Kang D, et al. (2017) Precise stacking of decellularized extracellular matrix based 3D cell-laden constructs by a 3D cell printing system equipped with heating modules. *Sci Rep* 7(1).
76. Lee M, Bae K, Levinson C, Zenobi-Wong M (2020) Nanocomposite bioink exploits dynamic covalent bonds between nanoparticles and polysaccharides for precision bioprinting. *Biofabrication* 12(2): 025025.
77. Ouyang L, Highley CB, Rodell CB, Sun W, Burdick JA (2016) 3D Printing of Shear-Thinning Hyaluronic Acid Hydrogels with Secondary Cross-Linking. *ACS Biomater Sci Eng* 2(10): 1743-1751.
78. Comeau PA, Willett TL (2020) Triethyleneglycol dimethacrylate addition improves the 3D-printability and construct properties of a GelMA-nHA composite system towards tissue engineering applications. *Mater Sci Eng C*: 112, 110937.
79. Li H, Tan YJ, Liu S, Li L (2018) Three-Dimensional Bioprinting of Oppositely Charged Hydrogels with Super Strong Interface Bonding. *ACS Biomater Sci Eng* 10(13): 11164-11174.
80. Paxton N, Smolan W, Böck T, Melchels F, Groll J, et al. (2017) Proposal to assess printability of bioinks for extrusion-based bioprinting and evaluation of rheological properties governing bioprintability. *Biofabrication* 9(4): 044107.
81. Diamantides N, Wang L, Puijksma T, Siemiatkoski J, Dugopolski, et al. (2017) Correlating rheological properties and printability of collagen bioinks: the effects of riboflavin photocrosslinking and pH. *Biofabrication* 9(3): 034102.
82. Hu W, Wang Z, Xiao Y, Zhang S, Wang J (2019) Advances in crosslinking strategies of biomedical hydrogels. *Biomater Sci* 7(3): 843-855.
83. Chen CW, Betz MW, Fisher JP, Paek A, Chen Y (2011) Macroporous Hydrogel Scaffolds and Their Characterization by Optical Coherence Tomography. *Tissue Eng Part C Methods* 17(1): 101-112.
84. Tan W, Oldenburg AL, Norman JJ, Desai TA, Boppart SA (2006) Optical coherence tomography of cell dynamics in three-dimensional tissue models. *Opt Express* 14(16): 7159.
85. Benninger, RKP, Piston, DW (2013) Two-Photon Excitation Microscopy for the Study of Living Cells and Tissues. *Curr Protoc Cell Biol* 59(1): 4.11.1-4.11.24.
86. Liu B, Li J, Lei X, Cheng P, Song Y, et al. (2020) 3D-bioprinted functional and biomimetic hydrogel scaffolds incorporated with nanosilicates to promote bone healing in rat calvarial defect model. *Mater Sci Technol* 112: 110905.
87. Xu W, Molino BZ, Cheng F, Molino PJ, Yue Z, et al. (2019) On Low-Concentration Inks Formulated by Nanocellulose Assisted with Gelatin Methacrylate (GelMA) for 3D Printing toward Wound Healing Application. *ACS Appl Mater Interfaces* 11(9): 8838-8848.
88. Gao Q, Niu X, Shao L, Zhou L, Lin Z, et al. (2019) 3D printing of complex GelMA-based scaffolds with nanoclay. *Biofabrication* 11(3): 035006.
89. Schütz K, Placht AM, Paul B, Brüggemeier S, Gelinsky M, et al. (2015) Three-dimensional plotting of a cell-laden alginate/methylcellulose blend: towards biofabrication of tissue engineering constructs with clinically relevant dimensions. *J Tissue Eng Regen Med* 11(5): 1574-1587.

90. Bao M, Xie J, Huck WTS (2018) Recent Advances in Engineering the Stem Cell Microniche in 3D. *Adv Sci* 5(8): 1800448.
91. Wang N, Tytell JD, Ingber DE (2009) Mechanotransduction at a distance: mechanically coupling the extracellular matrix with the nucleus. *Nat Rev Mol Cell Biol* 10(1): 75-82.
92. Galbraith CG, Sheetz MP (1998) Forces on adhesive contacts affect cell function. *Current Opinion in Cell Biology* 10(5): 566-571.
93. Iskratsch T, Wolfenson H, Sheetz MP (2014) Appreciating force and shape – the rise of mechanotransduction in cell biology. *Nat. Rev Mol Cell Biol* 15(12): 825-833.
94. Critchley DR (2000) Focal adhesions – the cytoskeletal connection. *Curr Opin Cell Biol* 12(1): 133-139.
95. Dupont S, Morsut L, Aragona M, Enzo E, Giulitti S, et al. (2011) Role of YAP/TAZ in mechanotransduction. *Nature*, 474(7350): 179-183.
96. Gupta M, Sarangi BR, Deschamps J, Nematbakhsh Y, Callan-Jones A, et al. (2015) Adaptive rheology and ordering of cell cytoskeleton govern matrix rigidity sensing. *Nat. Commun* 25(6): 7525.
97. Wong S, Guo WH, Wang YL (2014) Fibroblasts probe substrate rigidity with filopodia extensions before occupying an area. *Proceedings of the National Academy of Sciences* 111(48): 17176-17181.
98. Yang C, DelRio FW, Ma H, Killaars AR, Basta LP, et al. (2016) Spatially patterned matrix elasticity directs stem cell fate. *PNAS* 113(31): E4439-E4445.
99. Elosegui-Artola A, Andreu I, Beedle A, Lezamiz A, Uroz M, et al. (2017) Force Triggers YAP Nuclear Entry by Regulating Transport across Nuclear Pores. *Cell* 171(6): 1397–1410.e14.
100. Vedula, SRK, Leong MC, Lai TL, Hersen P, Kabla AJ, et al. (2012) Emerging modes of collective cell migration induced by geometrical constraints. *PNAS* 109(32): 12974-12979.
101. Kim J, Feng J, Jones CAR, Mao X, Sander, et al. (2017) Stress-induced plasticity of dynamic collagen networks. *Nat Commun* 8(1).
102. Wolf K, Te Lindert M, Krause M, Alexander S, Te Riet, et al. (2013) Physical limits of cell migration: control by ECM space and nuclear deformation and tuning by proteolysis and traction force. *J Cell Biol* 201(7): 1069-1084.
103. Babaei B, Abramowitch SD, Elson EL, Thomopoulos S, Genin GM, et al. (2015) A discrete spectral analysis for determining quasi-linear viscoelastic properties of biological materials. *J R Soc Interface* 12(113): 20150707.
104. Park YD, Tirelli N, Hubbell JA (2003) Photopolymerized hyaluronic acid-based hydrogels and interpenetrating networks. *Biomaterials* 24(6): 893-900.
105. Zhao X, Huebsch N, Mooney DJ, Suo Z (2010) Stress-relaxation behavior in gels with ionic and covalent crosslinks. *J Appl Phys* 107(6): 063509.
106. Müller C, Müller A, Pompe T (2013) Dissipative interactions in cell–matrix adhesion. *Soft Matter* 9(27): 6207.
107. Kraning-Rush M, Carey SP, Lampi MC, Reinhart-King CA (2013) Microfabricated collagen tracks facilitate single cell metastatic invasion in 3D. *Integr Bio* 5(3): 606-16.
108. Stroka, Kimberly M, Jiang H, Chen SH, Tong Z, et al. (2014) Water Permeation Drives Tumor Cell Migration in Confined Microenvironments. *Cell* 157(3): 611-623.
109. Liu, YJ, Le Berre, M, Lautenschlaeger, F, Maiuri, P, Callan-Jones, et al. (2015) Confinement and Low Adhesion Induce Fast Amoeboid Migration of Slow Mesenchymal Cells. *Cell* 160(4): 659-672.
110. Rolli CG, Seufferlein T, Kemkemer R, Spatz JP (2010) Impact of Tumor Cell Cytoskeleton Organization on Invasiveness and Migration: A Microchannel-Based Approach. *PLoS ONE* 5(1): e8726.
111. Warmflash A, Sorre B, Etoc F, Siggia ED, Brivanlou AH, et al. (2014) A method to recapitulate early embryonic spatial patterning in human embryonic stem cells. *Nat Methods* 11(8): 847–854.
112. Tan KY, Lin H, Ramstedt M, Watt FM, Huck WTS, et al. (2013) Decoupling geometrical and chemical cues directing epidermal stem cell fate on polymer brush-based cell micro-patterns. *Integrative Biology* 5(6): 899-910.
113. Werner M, Blanquer SBG, Haimi SP, Korus G, Dunlop JWC, et al. (2016) Surface Curvature Differentially Regulates Stem Cell Migration and Differentiation via Altered Attachment Morphology and Nuclear Deformation. *Adv Sci* 4(2): 1600347.
114. Connelly JT, Gautrot JE, Trappmann B, Tan DWM, Donati G, et al. (2010) Actin and serum response factor transduce physical cues from the microenvironment to regulate epidermal stem cell fate decisions. *Nat Cell Biol* 12(7): 711-718.
115. Von Erlach TC, Bertazzo S, Wozniak MA, Horejs CM, Maynard SA, et al. (2018) Cell-geometry-dependent changes in plasma membrane order direct stem cell signalling and fate. *Nat Mater* 17(3): 237-242.
116. McBeath R, Pirone DM, Nelson CM, Bhadriraju K, Chen CS (2004) Cell Shape, Cytoskeletal Tension, and RhoA Regulate Stem Cell Lineage Commitment. *Dev Cell* 6(4): 483-495.
117. Chen CS, Mrksich M, Huang S, Whitesides GM, Ingber DE (1998) Micropatterned Surfaces for Control of Cell Shape, Position, and Function. *Biotechnol Prog* 14(3): 356-363.
118. Ihalainen TO, Aires L, Herzog FA, Schwartlander R, Moeller J, et al. (2015) Differential basal-to-apical accessibility of lamin A/C epitopes in the nuclear lamina regulated by changes in cytoskeletal tension. *Nat Mater* 14(12): 1252-1261.
119. Desai RA, Khan MK, Gopal SB, Chen CS (2011) Subcellular spatial segregation of integrin subtypes by patterned multicomponent surfaces. *Integr Biol* 3(5): 560.
120. Nelson CM, Jean RP, Tan JL, Liu WF, Sniadecki NJ, et al. (2005) Emergent patterns of growth controlled by multicellular form and mechanics *PNAS* 102(33): 11594-11599.
121. Vignaud T, Blanchoin L, Théry M (2012) Directed cytoskeleton self-organization. *Trends in Cell Biology* 22(12): 671-682.
122. Théry M, Racine V, Piel M, Pépin A, Dimitrov A, et al. (2006) Anisotropy of cell adhesive microenvironment governs cell internal organization and orientation of polarity. *PNAS* 103(52): 19771-19776.
123. Murrell M, Oakes PW, Lenz M, Gardel ML (2015) Forcing cells into shape: the mechanics of actomyosin contractility. *Nat Rev Mol Cell Biol* 16(8): 486-498.
124. Ron A, Azeloglu EU, Calizo RC, Hu M, Bhattacharya S, et al. (2017) Cell shape information is transduced through tension-independent mechanisms. *Nat Commun* 8(1):2145.

125. Watanabe T, Noritake J, Kaibuchi K (2005) Regulation of microtubules in cell migration. *Trends in Cell Biology* 15(2): 76-83.
126. Irianto J, Pfeifer CR, Bennett RR, Xia Y, Ivanovska IL, et al. (2016) Nuclear constriction segregates mobile nuclear proteins away from chromatin. *Mol Biol Cell* 27(25): 4011-4020.
127. Bruekers SMC, Bao M, Hendriks JMA, Mulder KW, Huck WTS, et al. (2017) Adaptation trajectories during adhesion and spreading affect future cell states. *Sci Rep* 7(1):12308.